Available online at www.sciencedirect.com
SCIENCE DIRECT®
Control Engineering Practice 13 (2005) 789–803
CONTROL ENGINEERING PRACTICE
www.elsevier.com/locate/conengprac

Nonlinear robust control of a hydraulic elevator: experiment-based modeling and two-stage Lyapunov redesign

Chang-Sei Kim[a], Keum-Shik Hong[b,*], Moon-Ki Kim[c]

[a]Robot Research and Development Team, Daewoo Shipbuilding and Marine Engineering, Ltd., Geoje-si, Gyeongsangnam-do 656-714, Korea
[b]School of Mechanical Engineering, Pusan National University, San 30, Jangjeon-dong, Gumjung-gu, Busan 609-735, Korea
[c]Department of Mechanical and Industrial Engineering, University of Massachusetts Amherst, Amherst, MA 01003, USA

Received 23 August 2003; accepted 6 September 2004
Available online 19 October 2004

Abstract

In this paper, a robust velocity control problem for hydraulic elevators is investigated. The analysis is divided into two parts, mechanical and hydraulic. A detailed mathematical model for the mechanics is established for the purpose of simulation, but the control system design is carried out with a simplified model reduced from the detailed one. The three important characteristics of a hydraulic elevator, including cylinder friction, pump friction, and pump leakage, are modeled through experiments. The leakage property is characterized as a function of temperature and pressure. A two-stage nonlinear robust controller using the Lyapunov redesign method is established for velocity tracking control. At the first stage, a robust controller for the mechanical part is designed to yield the desired cylinder pressure for reference velocity tracking. At the second stage, a robust controller for the hydraulic part is designed to track the reference pressure generated from the first controller. Simulation results validate that the proposed method is robust in the presence of nonlinearities and uncertainties.

Keywords: Hydraulic elevator; Control system design; Lyapunov redesign; Friction; Leakage; Stability; Robustness

1. Introduction

There are two types of elevator systems depending on the actuation mechanism: a roped elevator and a hydraulic elevator. The roped elevator is driven by a rope and an electric motor, while the hydraulic elevator is driven by a cylinder and fluid power. The assembly of the car, rope and pulley of a hydraulic elevator is similar to that of a roped elevator. But, the up and down movement of the car of a hydraulic elevator is achieved by the pushing and pulling of the pulley hooked at the end of a hydraulic jack, whereas that of a roped elevator is achieved by the winding and unwinding of the rope on a drum.

The hydraulic elevator is cost-effective and makes for very clean lines of building exterior due to the elimination of the conventional penthouse-type machine room. Since hydraulic circuits can be inserted anywhere inside a building, possible sun blocking due to building extensions can be avoided. Particularly, to secure pedestrians' space and improve the appearance of a street, the installation of hydraulic elevators at subways, pedestrian crossings, and in low-level buildings is increasing. The use of hydraulic elevators is especially promising in low-level buildings such as airports and low-rise houses. It has been reported that since 1990 the market share of hydraulic elevators has been over 35% (Sedrak, 2000).

The control scheme of a hydraulic elevator consists of three control steps: the load pressure compensation step,

*Corresponding author. Tel.: +82 51 510 2454; fax: +82 51 514 0685.
E-mail addresses: cskim5@dsme.co.kr (C.-S. Kim), kshong@pusan.ac.kr (K.-S. Hong), mkim@titan.me.jhu.edu (M.-K. Kim).

0967-0661/$ - see front matter © 2004 Elsevier Ltd. All rights reserved.
doi:10.1016/j.conengprac.2004.09.003

the velocity tracking control step, and the destination position control step. The load pressure compensation step reduces the jolt at the departure of the car that may produce an uncomfortable ride for passengers. The velocity tracking control makes the car follow a reference velocity profile that helps the passengers feel comfortable during the movement. The destination position control reduces the position error, which may exist after the velocity tracking control, at the target position.

A hydraulic pump connected directly to an electric motor generates fluid power and controls the velocity of the car. A smooth transition of car depends on the smooth movement of the cylinder. However, the following problems occur: (1) The system characteristics change due to the variations of the load and oil temperature; (2) jolts occur due to unequal pressures at the departure and arrival points; (3) an undesirable descent occurs due to oil leakage; and (4) unknown nonlinearities in the friction and continuity equations appear. These problems will eventually degrade the safety and comfort of the passengers (Nakamura, 2000).

In this paper, the velocity control problem of hydraulic elevators is investigated (Jianmin, 2000; Kang & Kim, 2000; Li, 2001; Sha, Bajic, & Yang, 2002; Teramoto & Nakamura, 1997). Sha et al. (2002) has introduced a new approximated linear model for a hydraulic elevator and investigated a sliding mode control for velocity tracking in the discrete domain. Teramoto and Nakamura (1997) has introduced a third-order linearized model with fixed parameters, for which their open-loop experiments showed that the effects of nonlinearities and uncertainties were too large to describe the system behavior sufficiently.

To solve these problems, the hydraulic elevator system was divided into two facets: a mechanical facet that includes the car, rope, and pulleys, and a hydraulic facet that includes the cylinder, logic valve, hydraulic power unit, and pipes. Then, the dynamic equations for each facet are derived. The mathematical model of the mechanics is a 14th-order linear equation including all the pulleys and rope dynamics, whereas the mathematical model of the hydraulics is expressed as a set of nonlinear equations with uncertainties, that is, flow equations and continuity equations. Kim (2000) revealed that the open-loop simulation results of the mathematical models reported in the literature were inconsistent with open-loop experimental results. Thus, a series of experiments have been performed to obtain more accurate mathematical models for the frictions in the hydraulic cylinder and pump (Armstrong-Helouvry, Dupont, & Wit, 1994; Bo & Pavelescu, 1982; Karnopp, 1985). In addition, the leakage coefficient has been modeled as a function of temperature and pressure in the hydraulic equation.

Recently, many nonlinear robust control methods have been proposed: sliding mode control (Bouri & Thomasset, 2001; Wheeler, Su, & Stepanenko, 1998), the back-stepping method (Krstic, Kanellakopulos, & Kokotovic, 1995), and the Lyapunov redesign method (Kim, Lee, & Cho, 2002; Qu, 1998). Also, numerous applications of the robust control methods for nonlinear systems with uncertainty have been reported (Alleyne, 1996; Sohl & Bobrow, 1999; Yanada & Shimahara, 1997; Yao, Fanping, Reedy, & Chiu, 2000; Corless & Leitmann, 1997; Venkatesh, Cho, & Kim, 2002; Michino, Mizumoto, Iwai, & Kumon, 2003; Kwon, Han, & Ahn, 2004). Alleyne (1996) proposed a variant of the backstepping method and improved the force tracking performance of an electro-hydraulic actuator. To compensate for the parameter uncertainty of a nonlinear cement mill model, Grognard, Jadot, Magni, Bastin, Sepulehre, and Wertz (2001) designeda Lyapunov-function-based controller. Yao et al. (2000) suggested a discontinuous projection-based adaptive robust controller for a single-rod hydraulic cylinder with constant unknown inertia load. Sha et al. (2002) used a discrete adaptive sliding mode control for a hydraulic elevator velocity tracking system.

To improve the efficiency of the elevator system, we propose a two-stage nonlinear robust controller, using the Lyapunov redesign method, for the velocity control of the hydraulic elevator system. At the first stage, a robust controller for the mechanics is synthesized to control the velocity of the car. The control input to the mechanics is used as a reference to the subsequent pressure tracking control. At the second stage, another robust controller for the hydraulics is designed for the purpose of tracking the reference pressure generated from the first controller. The proposed method showed good control performance in the presence of uncertainties.

The paper is structured as follows. In Section 2, the derived mathematical models of the mechanical and hydraulic facets of the hydraulic elevator system considered are presented. In Section 3, a cylinder friction model, a hydraulic pump friction model, and the leakage characteristics of the pump, constructed through a series of experiments, are explained. The controller design, using a two-stage Lyapunov redesign method, is presented in Section 4. In Section 5, the simulation results of the velocity control using the proposed models are shown. Conclusions are given in Section 6.

2. System modeling: dynamics

The equations of motion of the mechanics and hydraulics presented in this section are, respectively, derived from classical Newtonian dynamics, the continuity equation, and the flow equation.

2.1. Mechanics

The mechanics consist of a passenger car (cabin) in which the passengers ride, a hydraulic cylinder, ropes,

and pulleys. Fig. 1 depicts a schematic of the considered hydraulic elevator system and detailed modeling of its mechanical parts. Each rope segment is modeled as a spring and damper system.

Let x_c be the vertical displacement of the car; let x_j be the vertical displacement of the hydraulic jack; let $f_j(\dot{x}_j, x_j)$ be the friction in the hydraulic cylinder which is a nonlinear function of velocity and displacement in general; let P_j be the pressure in the hydraulic cylinder let θ_{c1} and θ_{c2} be the rotation angles of the two wheels of the car as shown in Fig. 1; θ_{j1}, θ_{j2}, and let θ_{j3} be the rotation angles of the pulleys, respectively. The parameter values used in the simulation are displayed in Table 1.

In this detailed model, the state vector X_f is defined as $X_f = [x_j\ \dot{x}_j\ x_c\ \dot{x}_c\ \theta_{c2}\ \dot{\theta}_{c2}\ \theta_{j1}\ \dot{\theta}_{j1}\ \theta_{j2}\ \dot{\theta}_{j2}\ \theta_{j3}\ \dot{\theta}_{j3}]$. Also, the equations of motion of the mechanics are

$$\dot{X}_f = A_f X_f + B_f u_f + \Delta f_f, \tag{1}$$

where $A_f \in R^{14\times 14}$, $B_f = [0 A_j/M_j 0 \ldots 0]^{\mathrm{T}} \in R^{14\times 1}$, $\Delta f_f = [0 f_j(\dot{x}_j, x_j)\ 0 \ldots 0]^{\mathrm{T}} \in R^{14\times 1}$ is the friction term, and $u_f = P_j$. See Appendix A for a complete description of A_f.

For the purpose of designing a control system, the detailed model of (1) is too complicated. Hence, a new control-oriented model that is much simpler than (1) is pursued. However (1), representing the plant dynamics, will be used in computer simulations at a later stage. Now, Fig. 1 is simplified to Fig. 2 under the assumption that the entire rope can be modeled as a 1-DOF element and the rope mass can be neglected.

Then, the dynamic equations of the simplified model are

$$\begin{aligned} M_j\ddot{x}_j = &-8C_{eq}(2\dot{x}_j - \dot{x}_c) - 8K_{eq}(2x_j - x_c) \\ &+ f_j(\dot{x}_j, x_j) + A_j P_j, \end{aligned} \tag{2}$$

$$M_c\ddot{x}_c = -4C_{eq}(\dot{x}_c - 2\dot{x}_j) - 4K_{eq}(x_c - 2x_j) - C_c\dot{x}_c, \tag{3}$$

where C_{eq} is the equivalent damping constant of the rope ($11.525e^3$ N s/m) and K_{eq} is the equivalent spring constant of the rope ($667.664e^4$ N/m). The friction force $f_j(\dot{x}_j, x_j)$ was estimated from the experiments described in Section 3.1.

2.2. Hydraulics

Fig. 3 shows the hydraulic circuit of the elevator system considered, in which a logic valve, that is, the main check valve (MCV), is used for the safety of the system. Fig. 4 is a schematic of the MCV. Two solenoid valves associated with the MCV determine the up and down movements of the car by switching the oil-flow direction. In Fig. 5, the control logic and operation principle of this module are depicted. When both solenoid valves 1 and 2 are off, the hydraulic circuit performs an up-movement. If we increase the flow from the pump by increasing the input current to the motor, the spool of the logic valve opens. At this moment, the oil flows into the cylinder and the cylinder pressure increases. The increased cylinder pressure pushes up the hydraulic jack and lifts up the car. If both solenoid

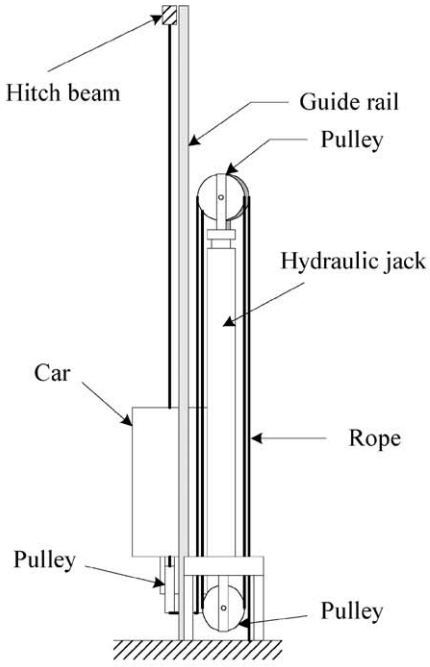

(a) Schematic of a hydraulic elevator.

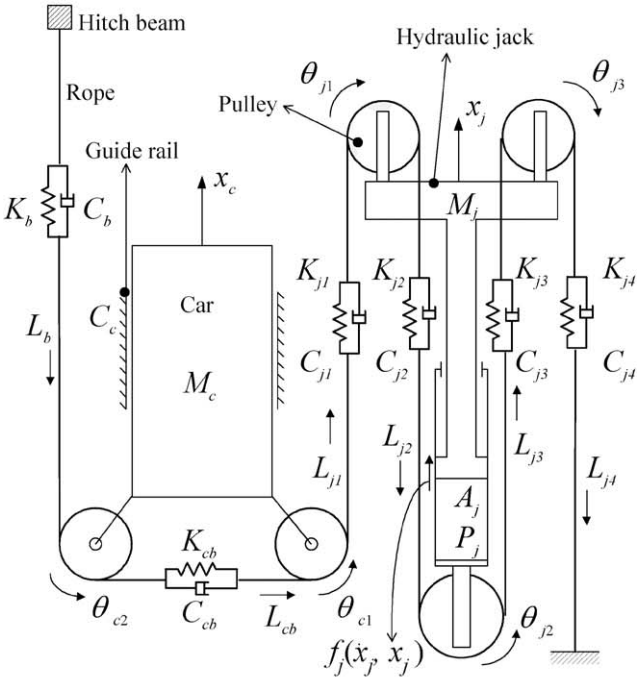

(b) A detailed model of the mechanics.

Fig. 1. Schematic of a hydraulic elevator and a detailed model of the mechanics: Each rope segment is modeled as a spring–damper system. (a) Schematic of a hydraulic elevator. (b) A detailed model of the mechanics.

Table 1
Physical parameters of mechanics

Name/signification	Symbol	Nominal value	Unit
Cross-sectional area of the piston in the hydraulic jack	A_j	0.0248846	m^2
Viscous friction between the car and guide rail	C_c	$3.617e^2$	N s/m
Damping constant of lower rope	C_{cb}	See (A.2) in Appendix A	N s/m
Damping constant of each rope	$C_{j1...4}$	See (A.2) in Appendix A	N s/m
Spring constant of lower rope	K_{cb}	See (A.2) in Appendix A	N/m
Spring constant of each rope	$K_{j1...4}$	See (A.2) in Appendix A	N/m
Mass of thecar	M_c	2000	kg
Mass of the hydraulic jack	M_j	188	kg

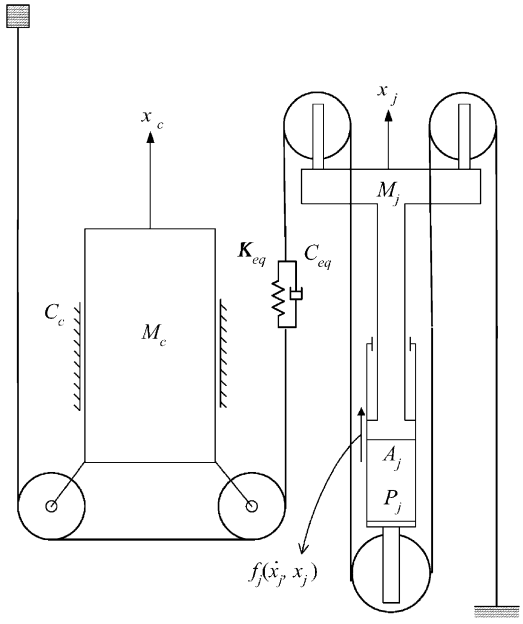

Fig. 2. A simplified model of the mechanics: The entire rope is modeled as a single spring–damper system.

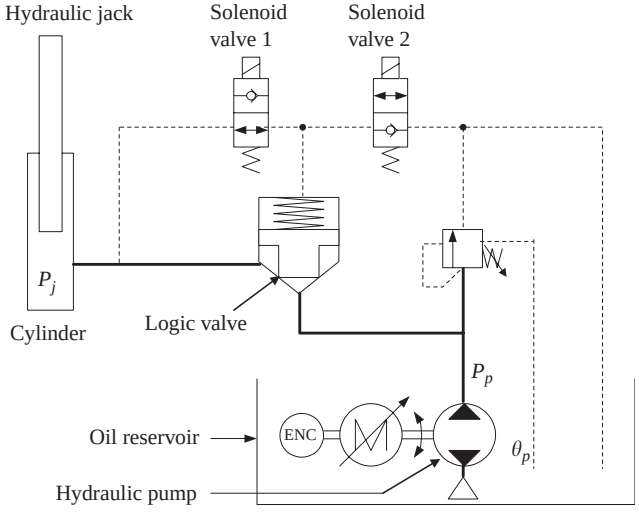

Fig. 3. The hydraulic circuit of the considered elevator system.

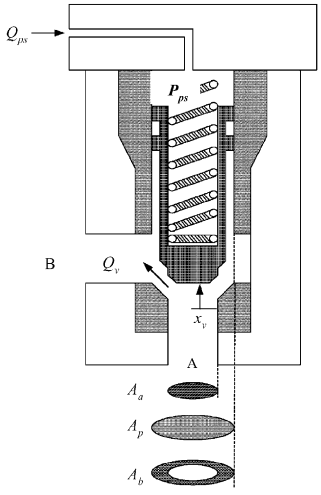

Fig. 4. Cross-sectional view of the logic valve.

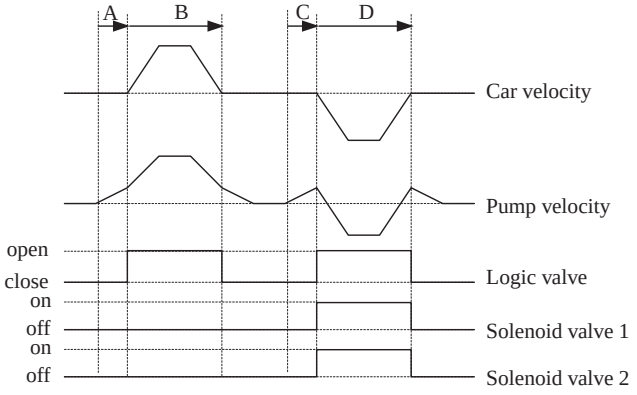

Fig. 5. Control logic: A and B are the load pressure compensation step and the velocity control step for an upward movement, respectively, while C and D are those for a downward movement.

valves 1 and 2 are on, the hydraulic circuit switches to perform a down movement. If we decrease the flow from the pump by reducing the input current to the pump, the spool of the logic valve opens and the oil in the cylinder outlets to the oil reservoir. And the hydraulic jack moves downward and thus the car moves down.

Let i_q be the input current to the pump; let T_m be the output torque of the pump; let θ_p be the angular displacement of the pump; let P_p be the pump pressure; let P_j be the cylinder pressure; let Q_p be the flow in the pump; let Q_v be the flow in the logic valve; let x_v be the displacement of the logic valve spool; and let $A(x_v)$ be the opening area of the MCV that is proportional to the spool displacement. The parameter values of the hydraulics are displayed in Table 2.

The relationship between the input current and the pump torque is given as

$$T_m = K_m i_q. \tag{4}$$

Then, the equation of motion of the pump is

$$J_{mp}\ddot{\theta}_p + C_p\sqrt{v}\dot{\theta}_p + D_p P_p + T_f = T_m, \tag{5}$$

where T_f is the pump friction which will be estimated by experiments (see Section 3.2). The flow equation and the continuity equation for the pump are given as

$$Q_p = D_p\dot{\theta}_p - \frac{C_l}{\sqrt{v}}P_p \tag{6}$$

and

$$\dot{P}_p = \frac{\beta}{V_p}(Q_p - Q_v). \tag{7}$$

The continuity equation between the logic valve and the cylinder is given as

$$\dot{P}_j = \frac{\beta}{V_{j0} + A_j x_j}(Q_v - A_j\dot{x}_j). \tag{8}$$

For the logic valve, the dynamic equation and the flow equation are

$$M_v\ddot{x}_v = P_j A_a + P_p A_b - P_{ps}A_p - C_v\dot{x}_v - K_v x_v, \tag{9}$$

$$Q_v = C_d A(x_v)\mathrm{sgn}(P_p - P_j)\sqrt{\frac{2|P_p - P_j|}{\rho}}, \tag{10}$$

where

$$A(x_v) = \frac{763 \times 10^{-6}}{9.2 \times 10^{-3}}\, x_v.$$

$A(x_v)$ is the opening area through which the oil flows from area A to area B shown in Fig. 4. This value is normally obtained from the data-sheet of the logic valve provided by the manufacturer. Because the response time of the logic valve is very fast compared with other dynamics, its dynamics is ignored in this context.

3. Friction and leakage models: experiment

Fig. 6 shows a downward movement open-loop experiment, which depicts the relationship between the input current, cylinder pressure, and car velocity. As seen in Fig. 6, even if we decrease the input current by −5 A/s up to 5 s, the cylinder pressure and car velocity do not change. Specifically, when the input current drops to 34 A, the cylinder pressure begins to change after 5 s, and the car begins to move down after 8.2 s. Hence, the region in which the cylinder pressure is not affected by the change of current input is called the first dead zone, and the following region in which the car velocity is not affected by the change of cylinder pressure is called the secondary dead zone. In Fig. 6, the first dead zone is from 2.4 to 5 s and the secondary one is from 5 to 8.2 s.

The first dead zone is known to occur due to pump friction and the leakage characteristics. And the secondary dead zone is due to cylinder friction. These

Table 2
Physical parameters of hydraulics

Name/signification	Symbol	Nominal value	Unit
Area of the logic valve flow in Fig. 5	A_b	4.61	cm^2
Area of the logic valve spool in Fig. 5	A_a	9.24	cm^2
Area of the logic valve in Fig. 5	A_p	13.85	cm^2
Discharging coefficient of the logic valve	C_d	0.6	
Leakage coefficient	C_l	$9.524e^{-10}$	
Viscosity coefficient of the pump	C_p	$5.333e^{-3}$	
Damping constant of the logic valve	C_v	0.0	N s/mm
Discharge coefficient	D_p	$3.07333018e^{-5}$	m^3/rad
Moment of inertia of the pump	J_{mp}	0.03172	kg m^2
Motor constant	K_m	1	m^3/rad
Spring constant of the logic valve	K_v	0.14611693	N/mm
Mass of the logic valve spool	M_v	0.445	kg
Initial volume of the cylinder	V_{j0}	0.05481	m^3
Volume of pipe and fittings	V_p	0.005374	m^3
Density of the oil	ρ	868	kg/m^3
Bulk modulus of the oil	β	$1.345485291e^9$	N/m^2
Kinematic viscosity coefficient of the oil	v	61.7 (at 40 °C)	CSt

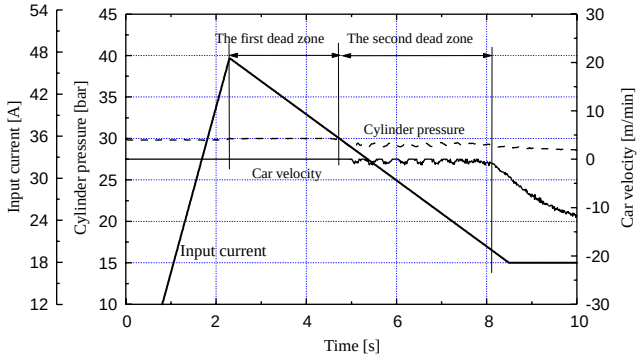

Fig. 6. Dead zone characteristics appearing in an open-loop experiment.

dead zones are a serious problem for the smooth maneuvering of the hydraulic elevator system.

To determine the characteristics of the dead zone and to complete the dynamic models shown in Section 2, three types of experiments were performed: a cylinder friction test, a pump friction test, and a pump leakage test.

To characterize the cylinder friction, we investigated a composite model of Bo and Pavelescu's friction model (1982) and Karnopp's friction model (1985). Bo and Pavelescu compared several friction models in the literature and proposed an exponential model of the form

$$F_f = F_c + (F_s - F_c)e^{-\alpha v} + F_v(v), \tag{11}$$

where F_c is the minimal level of Coulomb friction, F_s is the level of static friction, F_v is the viscous friction, v is the velocity, and α is an empirical parameter. Bo and Pavelescu's friction model is shown in Fig. 7. In addition to (11), to add static friction characteristics to the friction model, we adopted the Karnopp's friction model

$$F_f(\dot{x}, F) = \begin{cases} -\mathrm{sgn}(\dot{x})F_c & \text{if } |\dot{x}| > D_v, \\ -\mathrm{sgn}(F)\max(F, F_H) & \text{if } |\dot{x}| \leqslant D_v, \end{cases} \tag{12}$$

where D_v is a small neighborhood of zero velocity as shown in Fig. 8. By allowing friction within the interval $\pm D_v$, the integrator does not have to search for velocity-zero crossings (Armstrong-Helouvry et al., 1994).

3.1. Cylinder friction model

To obtain a cylinder friction model, experiments were performed under 12 different conditions. It was assumed that the maximal load and the operating range of the hydraulic elevator system considered are 1600 kg and a three-story building, respectively. Next, we set three different load conditions such as 0, 800, and 1600 kg. Also, four different operating situations were considered as follows: up from the 1st floor to the 2nd floor, up from the 2nd floor to the 3rd floor, down from the 3rd floor to the 2nd floor, and down from the 2nd floor to the 1st floor.

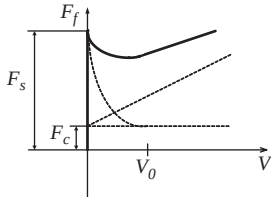

Fig. 7. Bo and Pavelescu's friction model (Bo & Pavelescu, 1982).

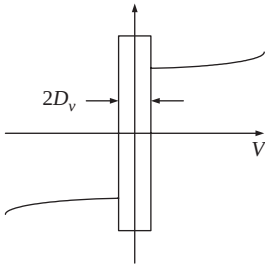

Fig. 8. Karnopp's friction model (Karnopp, 1985).

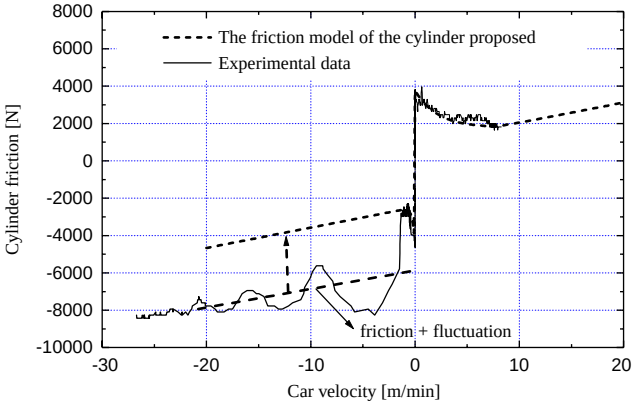

Fig. 9. Experimental data and the proposed friction model.

In Fig. 9, the solid line represents the experimental data of the cylinder friction with respect to the car velocity, and the dashed line represents that of the proposed friction model. Because the experimental data of a down movement contains not only the friction characteristics but also the fluctuations caused by the unequal pressure between the pump pressure and cylinder pressure, a gap between the experimental data and the proposed friction model does exist. Hence, the true cylinder friction could be obtained by eliminating the fluctuation effect from the experimental data (for more details, see Fig. 9). Finally, the friction model is proposed as

$$f_j(\dot{x}_j, x_j) = \begin{cases} -\mathrm{sgn}(\dot{x}_j)\{F_c + (F_s - F_c)e^{-\alpha\dot{x}_j} + C_j\dot{x}_j\} & \text{if } |\dot{x}_j| > D_v, \\ -\mathrm{sgn}(P_jA_j)\max(P_jA_j, F_s) & \text{if } |\dot{x}_j| \leqslant D_v, \end{cases} \tag{13}$$

Table 3
Parameters in the cylinder friction model (13)

	F_s(N)	F_c(N)	C_f(N s/m)	D_v(m/min)	α
Up motion	3875.6	1073.9	7230.5	1	0.47
Down motion	4344.7	1330.5	6727.3	0.6	9.94

where the parameter values of (13) are as displayed in Table 3. Each value was measured by averaging 12 different experimental results.

Two notable characteristics of the cylinder friction were observed from the experiments. First, the static friction is the dominant phenomenon causing a dead zone. As the hydraulic cylinder stands up, the weight of the car and load is added to the pressure of the cylinder and packing. This results in intensifying the friction phenomenon in the hydraulic cylinder. Second, the empirical parameter α in (11) is sensitive to the direction of car movement. Due to the car weight, we find a bigger value of the empirical parameter in a downward motion when compared with an upward motion. That is, the restoration time from the friction is relatively long when the elevator moves up against gravity and vice versa.

3.2. Pump friction model

The pump friction, T_f in (5), was estimated by experiments. To derive a pump friction equation, however, it is infeasible to measure the torque from the pump directly because the pump is inside the oil reservoir. We can, alternatively, estimate the pump torque using the relationship between the input current and the torque of the pump described in (4). In this study, $K_m = 1$ and $T_m = i_q$ were used.

Fig. 10 shows an experimental result of the pump itself under the condition that the input current increases at the rate of 2 A/s and the load pressure is 1 bar. A dead zone due to the pump friction appears from 0 to 4.3 s, at which the input current to the pump has reached approximately 8 A. Fig. 11 shows a comparison of the experimental data and the simulation results with the proposed model under no load. Two characteristics shown in Fig. 11 were observed: the viscosity changes when the angular velocity reaches near to 10 rpm, and the pump friction varies subject to the rotational direction of the pump. From this fact, we propose two friction models for each direction as a function of angular velocity.

When the pump rotates in the clockwise direction, for which we assign the negative value in this context, the pump friction is expressed as

$$\begin{aligned} T_f &= 3.7829\dot{\theta}_p && \text{if } -1 \leqslant \dot{\theta}_p < 0, \\ T_f &= 0.0036\dot{\theta}_p^2 + 0.1115\dot{\theta}_p + 3.6643 && \text{if } \dot{\theta}_p \leqslant -1, \end{aligned} \tag{14}$$

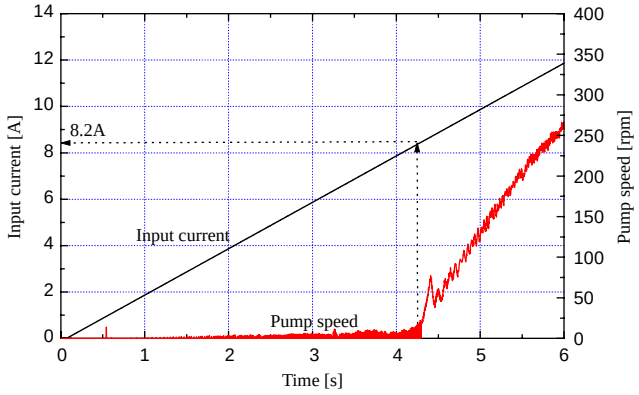

Fig. 10. Friction characteristics of the pump test.

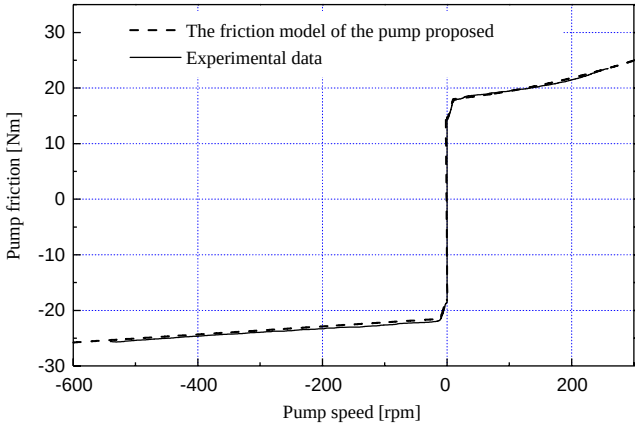

Fig. 11. The proposed friction model of the pump.

where $\dot{\theta}_p$ is the angular velocity of the pump and its unit is rad/s. Likewise, the pump friction under the counter-clockwise rotation is described as

$$\begin{aligned} T_f &= 3.4915\dot{\theta}_p && \text{if } 0 \leqslant \dot{\theta}_p < 1, \\ T_f &= 0.069\dot{\theta}_p - 3.4225 && \text{if } 1 \leqslant \dot{\theta}_p. \end{aligned} \tag{15}$$

3.3. Pump leakage model

In this experiment, the highest temperature in the reservoir is assumed to be 40 °C, whereas the lowest one is 10 °C. For each temperature, we varied the setting pressure of the relief valve from 0 to 35 bar to obtain a pump leakage model according to temperature and pressure.

Fig. 12 shows a schematic of the experimental setup and Fig. 13 is a picture of the setup. As shown in Fig. 12, after setting the relief valve pressure to a constant, we increase the input current to the motor until the pump pressure reaches the fixed relief valve pressure. Then, the pump speed reaches a steady state, as $\ddot{\theta}_p = 0$. At this time, if we close the relief valve, $Q_p = 0$ in (6) is achieved. Physically, in this state, there is no output flow of the pump. The pump is working only to compensate the leak flow and maintain the relief valve pressure in the pipe that connects the pump and valve block. Therefore, the following equation holds:

$$D_p\dot{\theta}_p = \frac{C_l}{\sqrt{v}} P_p. \tag{16}$$

By measuring the pump pressure, pump speed, and oil temperature, we established C_l as a function of pressure and temperature. The tests were repeated for various conditions of relief valve pressure and oil temperature.

Fig. 14 shows the experimental data sampled from the leakage tests, and, accordingly, the following leakage model is proposed in logarithmic form as a function of temperature and pressure:

$$C_l = \frac{C_{high}(P_p) - C_{low}(P_p)}{40 - 15}, \tag{17}$$

where $C_{high}(P_p) = -0.1577\mathrm{e}^{-8}\log_{10} P_p + 0.3373\mathrm{e}^{-8}$, $C_{low}(P_p) = -0.0687\mathrm{e}^{-8}\log_{10} P_p + 0.1806\mathrm{e}^{-8}$, and $C_{high}(P_p)$ is the leakage function for high-temperature oil and $C_{low}(P_p)$ is the leakage function for low-temperature oil. Since the logarithm of zero is undefined, an offset of 0.0001 is applied to P_p in this context.

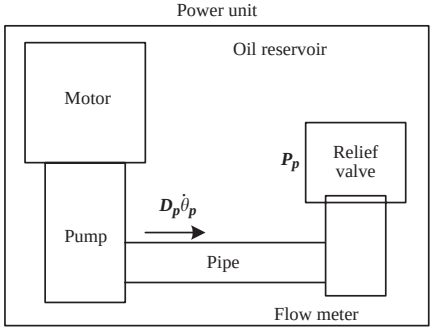

Fig. 12. Schematic of the experimental setup for testing pump leakage.

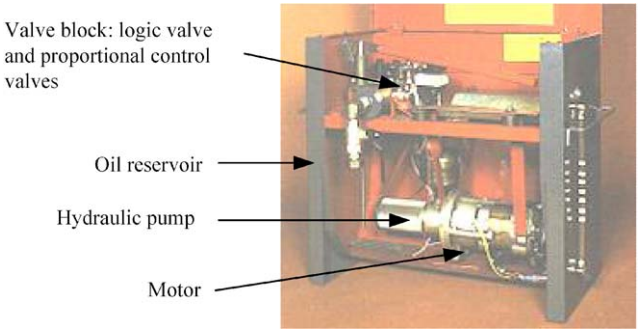

Fig. 13. The leakage experimental setup (LG Industrial Systems, Ltd., Korea).

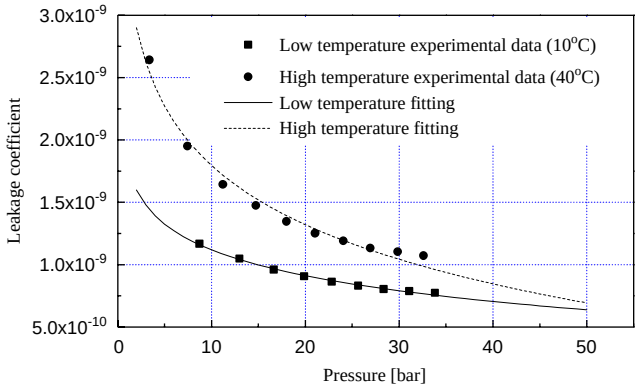

Fig. 14. Pump leakage experimental data and models.

All of the friction and leakage models developed here were verified by comparing them with the experimental results under the same input and load conditions. Fig. 15(a) and (b) demonstrate the similar behavior of the 4 states between the actual experimental results and the model-based simulation results using the same input current (5 A/s) for an upward movement. The impulse response of the mechanical facet, displayed in Fig. 15(c) and (d), confirm the validity of the simulation model.

4. Controller design

The Lyapunov redesign method can provide a solution to achieving robustness for a nonlinear system with uncertainties. One begins with a Lyapunov function for the nominal closed-loop system and then extends it to construct a controller that guarantees robustness to uncertainties.

Consider the following system:

$$\dot{x} = F(x,t) + G(x,t)u + \Delta(x,t), \tag{18}$$

where $x \in R^n$, $F(x,t) : R^n \times R \to R^n$, $G(x,t) : R^n \times R \to R^{n\times m}$, $u \in R^m$, and $\Delta(x,t) \in R^m$. Its error equation is defined as

$$\dot{e} = A(e,t) + B(e,t)\mu + B(e,t)\Delta(e,t), \tag{19}$$

where $e \in R^n$, $A(e,t) : R^n \times R \to R^n$, and $B(e,t) : R^n \times R \to R^{n\times m}$. Corless and Leitmann (1981) proposed the following state feedback control law for (19)

$$\mu(e,t) = \begin{cases} -\frac{p(e,t)}{\|p(e,t)\|}\rho(\cdot) & \text{if } \|p(e,t)\| > \varepsilon, \\ -\frac{p(e,t)}{\varepsilon}\rho(\cdot) & \text{if } \|p(e,t)\| \leqslant \varepsilon, \end{cases} \tag{20}$$

where $p(e,t) = B^{\mathrm{T}}(e,t)\frac{\partial V(e,t)}{\partial e}\rho(\cdot)$ and $\rho(\cdot)$ is a bound function of the system uncertainty $\Delta(e,t)$ in (19). For a given $\varepsilon > 0$ and $|\Delta(e,t)| \leqslant \rho(\cdot) + k|\mu|$, where μ is used as a

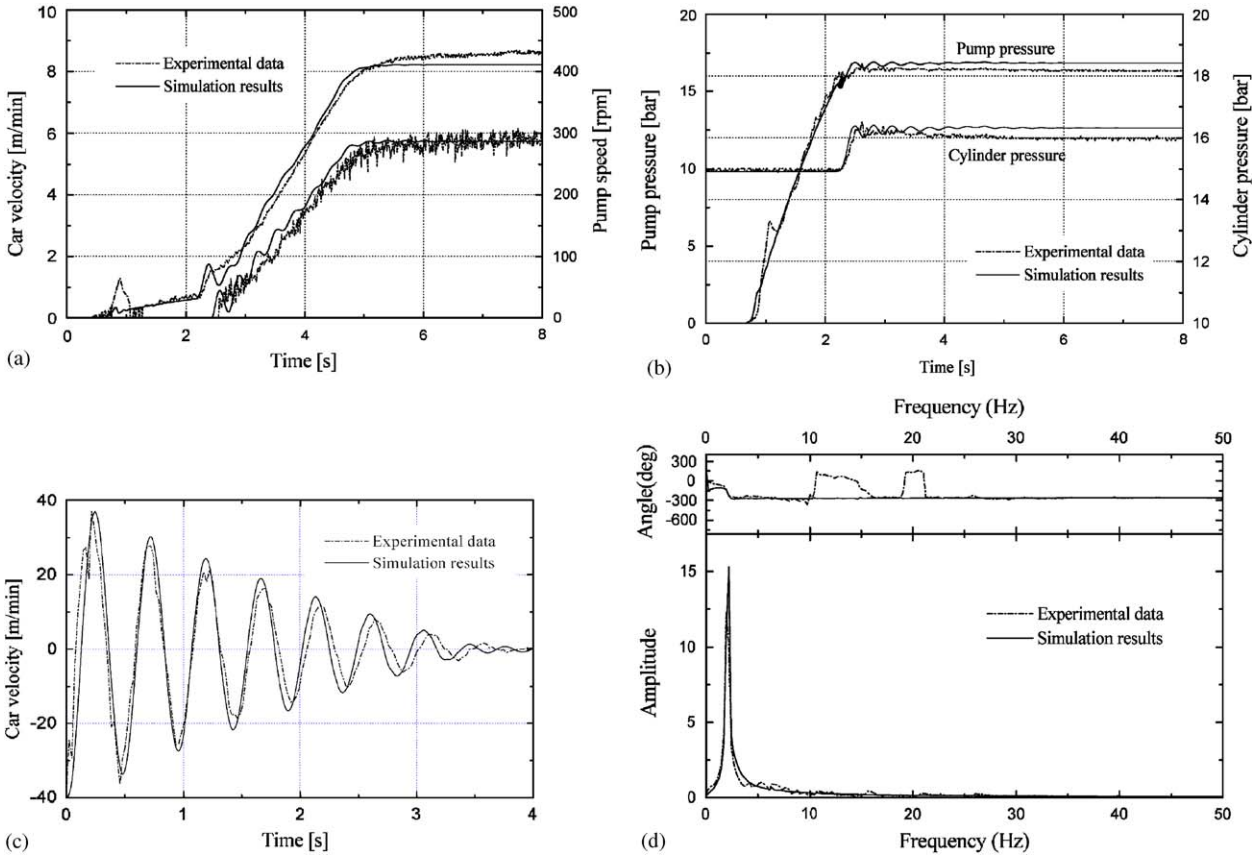

Fig. 15. Comparison between experimental data and simulation results: In (a) and (b), pump speed, pump pressure, cylinder pressure, and car velocity can represent the validity of the motor–pump model, the pump-cylinder equations including pump friction and leak flow, the cylinder and valve model, and the composite dynamics of the cylinder and the mechanics, respectively. In (c) and (d), the validity of the impulse response of the mechanics is displayed for both the time domain and the frequency domain. (a) Pump speed and car velocity: upward movement. (b) Pump pressure and cylinder pressure: upward movement. (c) Impulse response of the mechanics in the time domain: downward movement. (d) Impulse response of the mechanics in the frequency domain: downward movement.

robust input, the control (20) has been shown to guarantee the ultimate boundedness of all possible system responses within an arbitrarily small neighborhood of the zero state (by letting $\varepsilon \to 0$. Thus, a continuous control of (20) assures uniform asymptotic stability.

We investigated a two-stage robust controller for the mechanical and hydraulic facets of the hydraulic elevator. Fig. 16 shows a block diagram of the control algorithm. For the mechanics, we generated a reference pressure of the cylinder, P_j^d, using the car velocity reference, $\dot{x}_c^d$, and the car velocity feedback, $\dot{x}_c$. Then, for the hydraulics, using the cylinder pressure feedback, P_j, and the reference pressure, P_j^d, we generated the input current i_q of the hydraulic pump. for the hydraulic part.

Defining the state variables as $[x_1\,x_2\,x_3\,x_4\,x_5\,x_6\,x_7\,x_8\,x_9\,x_{10}]^{\mathrm{T}} = [x_c\,\dot{x}_c\,x_j\,\dot{x}_j\,P_j\,\dot{P}_j\,P_p\,\dot{P}_p\,\theta_p\,\dot{\theta}_p]^{\mathrm{T}}$ and $u_m = x_5$, (2)–(8) can be rewritten as

$$\dot{x}_2 = -a_1(x_2 - 2x_4) - a_2(x_1 - 2x_3), \tag{21}$$

$$\dot{x}_4 = -a_3(2x_4 - x_2) - a_4(2x_3 - x_1) - a_5x_4 + a_6f_c(x_3, x_4) + a_7u_m, \tag{22}$$

$$x_6 = -a_8x_4 - (a_9 + \Delta a_9)x_7 - a_{10}x_8 + a_{11}x_{10}, \tag{23}$$

$$\dot{x}_{10} = -a_{12}x_{10} - a_{13}x_7 - a_{14}T_f(x_9, x_{10}) + b_1(u_h + i_{res}), \tag{24}$$

where $a_1 = 4C_{eq}/(\Delta M_c + M_c)$, $a_2 = 4K_{eq}/(\Delta M_c + M_c)$, $a_3 = 8C_{eq}/M_j$, $a_4 = 8K_{eq}/M_j$, $a_5 = C_j/M_j$, $a_6 = 1/M_j$, $a_7 = A_j/M_j$, $a_8 = \beta A_j/V_j$, $a_9 = \beta C_l/(V_j\sqrt{v})$, $a_{10} = V_p/V_j$, $a_{11} = \beta D_p/V_j$, $a_{12} = C_p\sqrt{v}/J_{mp}$, $a_{13} = D_p/J_{mp}$, $a_{14} = 1/J_{mp}$, $b_1 = K_m/J_{mp}$, $f_c(x_3, x_4) = f_j(x_3, x_4) - C_jx_4$, and i_{res} is the residual input current in the pressure compensation stage due to the switching of the control mode from a pressure compensation problem to a velocity tracking problem. As the mass of the car, M_c, varies from 0 to 1600 kg, we assumed that the nominal value is 800 kg and $\Delta M_c \in [-800, 800]$. According to the sensitivity analysis of the nonlinear model of the hydraulic elevator system, the sensitive parameter

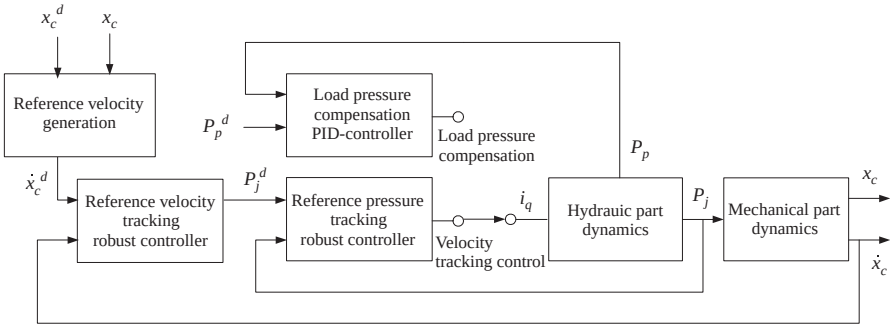

Fig. 16. Block diagram of a two-stage control of elevator car velocity.

affecting the velocity control is defined as $M_c(54\%) > C_j(31\%) > \beta(7\%)$. As the effect of the oil bulk modulus is relatively small, we considered the oil bulk modulus as a constant. The sensitivity analysis of a nonlinear system is well explained in Khalil (1992).

4.1. Mechanics: velocity tracking control

Using a kinematic constraint such as $x_1 = 2x_3 + \delta$ and parameters $a_1 \sim a_7$, (21) and (22) can be rewritten as

$$4(\Delta M_c + M_c)\dot{x}_2 + M_j(\dot{x}_2 - \ddot{\delta}) + C_j(x_2 - \dot{\delta}) + 2f_c(x_3, x_4) = 2A_j u_m, \tag{25}$$

where δ is a deformation value of the rope and u_m is the control input. The friction term $f_c(x_3, x_4)$ is the uncertainty that we have to cope with. Then, the nominal system equation becomes

$$(4M_c + M_j)\dot{x}_2 + C_j x_2 = 2A_j u_m. \tag{26}$$

Let the position error be $e_m = x_1^d - x_1$. Then, the error equation becomes

$$(4M_c + M_j)\ddot{e}_m + C_j\dot{e}_m = (4M_c + M_j)\dot{x}_2^d + C_j x_2^d - 2A_j u_m. \tag{27}$$

The control input to the mechanics of the hydraulic elevator system, u_m, is defined as $u_m = \varphi_m + k_m\mu_m$, where φ_m is a nominal control input and μ_m is a robust control input. The nominal control input of the mechanical part is defined as

$$\varphi_m = \frac{1}{2A_j}\left\{(4M_c + M_j)\dot{x}_2^d + C_j x_2^d + k_{m1}\dot{e}_m + k_{m2}e_m\right\}, \tag{28}$$

where k_{m1} is a derivative gain and k_{m2} is a proportional gain. Using an linear variable displacement transformer (LVDT), we could measure the state variables x_2 and $\dot{x}_2$. With the nominal control input $u_m = \varphi_m$, the error equation of the system is obtained as

$$(4M_c + M_j)\ddot{e}_m + (C_j + k_{m1})\dot{e}_m + k_{m2}e_m = 0. \tag{29}$$

We make (29) stable by selecting suitable gains k_{m1} and k_{m2}. And the system equation with uncertainties is rewritten as

$$(4M_c + M_j)\ddot{e}_m + (C_j + k_{m1})\dot{e}_m + k_{m2}e_m = 2A_j(-k_m\mu_m - \|\hat{f}_m\|), \tag{30}$$

where $\|\hat{f}_m\| = \frac{1}{2A_j}\left\|4\Delta M_c\dot{x}_2 - M_j\ddot{\delta} - C_j\dot{\delta} + 2f_c(x_3, x_4)\right\|_{\max}$.

To design a robust input, let the Lyapunov function and $p(e, t)$ be

$$V_m = \frac{1}{2}(e_m + k_m)^2 + \frac{1}{2}\dot{e}_m^2, \tag{31}$$

$$p(e, t) = \begin{bmatrix} 0 & -2A_j \end{bmatrix}\begin{bmatrix} e_m + k_m \\ \dot{e}_m \end{bmatrix}\rho(\cdot) = -2A_j\dot{e}_m\rho(\cdot), \tag{32}$$

where $\rho(\cdot) = \|\hat{f}_m\|$.

Since the stability of the control system in the case of $\|p(e, t)\| > \varepsilon$ is well established in (Corless & Leitmann, 1981; Khalil, 1992; Kim et al., 2002), we show the stability for the case of $\|p(e, t)\| \leqslant \varepsilon$ in (20). The derivative of the Lyapunov function (31) is given as

$$\begin{aligned}\dot{V}_m &= (e_m + k_m)\dot{e}_m + \dot{e}_m\ddot{e}_m \\ &= (e_m + k_m)\dot{e}_m - \dot{e}_m\frac{1}{4M_c + M_j}\{(C_j + k_{m1})\dot{e}_m \\ &\quad + k_{m2}e_m + 2A_j(\|\hat{f}_m\| + k_m\mu_m)\} \\ &= \left(1 - \frac{k_{m2}}{4M_c + M_j}\right)e_m\dot{e}_m + k_m\dot{e}_m - \frac{C_j + k_{m1}}{4M_c + M_j}\dot{e}_m^2 \\ &\quad - \frac{2A_j}{4M_c + M_j}(\|\hat{f}_m\| + k_m\mu_m)\dot{e}_m.\end{aligned} \tag{33}$$

The substitution of $\mu_m = -\frac{p(e,t)}{\varepsilon}\|\hat{f}_m\|$ into (33) yields

$$\begin{aligned}\dot{V}_m &= \left(1 - \frac{k_{m2}}{4M_c + M_j}\right)e_m\dot{e}_m \\ &\quad + \left(k_m - \frac{2A_j}{4M_c + M_j}\|\hat{f}_m\|\right)\dot{e}_m \\ &\quad - \left\{\frac{C_j + k_{m1}}{4M_c + M_j} + \frac{k_m}{\varepsilon}\frac{4A_j^2\|\hat{f}_m\|^2}{4M_c + M_j}\right\}\dot{e}_m^2.\end{aligned} \tag{34}$$

If we choose $k_{m2} = 4M_c + M_j$, $k_m = \frac{2A_j}{4M_c+M_j}\|\hat{f}_m\|$, $k_{m1} > 0$, and $\varepsilon = 0.02$, then the derivative of V_m becomes

$$\dot{V}_m = -\left\{\frac{C_j + k_{m1}}{4M_c + M_j} + \frac{k_m}{\varepsilon}\frac{4A_j^2\|\hat{f}_m\|^2}{4M_c + M_j}\right\}\dot{e}_m^2 \leqslant 0. \quad (35)$$

Finally, $V_m > 0$ and $\dot{V}_m \leqslant 0$ were proved, and the control input for the mechanics can be determined by the substitution of the computed gains into (20), (28), and (32).

4.2. Hydraulics: pressure tracking control

A robust controller for the hydraulics is designed to generate an input current that can track the cylinder reference pressure originating in the mechanics controller. Assume that

$$u_h = \varphi_h + k_h\mu_h + \frac{a_{13}}{b_1}x_7,$$

where φ_h is the nominal control input, μ_h is the robust control input, and $(a_{13}/b_1)x_7$ is the state feedback control of the hydraulics. For the convenience of calculation, define $g(x_4, x_7, x_8) = a_{10}x_8 + a_9x_7 + a_8x_4$. Here the states x_4, x_7, and x_8 are observable, so that $g(x_4, x_7, x_8)$ is a known function. The time derivative of (23) is given as

$$\dot{x}_6 = a_{11}\dot{x}_{10} - \dot{g}(x_4, x_7, x_8) - \Delta a_9\dot{x}_7. \quad (36)$$

The substitution of (24) into (36) yields

$$\begin{aligned}\dot{x}_6 = & -a_{11}a_{12}x_{10} - a_{11}a_{13}x_7 - a_{11}a_{14}T_f(x_9, x_{10}) \\ & + a_{11}b_1(u_h + i_{res}) - \dot{g}(x_4, x_7, x_8) - \Delta a_9\dot{x}_7. \end{aligned} \quad (37)$$

Assume that T_f is an uncertain function. The nominal system equation is

$$\begin{aligned}\dot{x}_6 = & -a_{11}a_{12}x_{10} - a_{11}a_{13}x_7 + a_{11}b_1(u_h + i_{res}) \\ & - \dot{g}(x_4, x_7, x_8). \end{aligned} \quad (38)$$

As we know that x_6^d is the derivative of the mechanics control input, u_m, we determine that the nominal control input for the hydraulics is φ_h, which is defined as

$$\begin{aligned}\varphi_h = & \frac{1}{a_{11}b_1}\{\dot{g}(x_4, x_7, x_8) + \dot{x}_6^d + a_{11}a_{13}x_7 + a_{11}a_{12}x_{10} \\ & + k_{h1}\dot{e}_h + k_{h2}e_h\} - i_{res}, \end{aligned} \quad (39)$$

where $e_h = x_5^d - x_5$. By applying $u_h = \varphi_h$ to (37), the error equation is obtained as

$$\ddot{e}_h^2 + k_{h1}\dot{e}_h + k_{h2}e_h = a_{11}b_1(-k_h\mu_h - \|\hat{f}_h\|), \quad (40)$$

where $\|\hat{f}_h\| = \frac{1}{a_{11}b_1}\|(a_{11}a_{14}T_f + \Delta a_9x_7)\|_{\max}$. And the Lyapunov function for the hydraulics is defined as

$$V_h = \frac{1}{2}(e_h + k_h)^2 + \frac{1}{2}\dot{e}_h^2. \quad (41)$$

We can also prove the stability of this function in the same manner as shown in Section 4.1. If we select $k_{h1} > 0$, $k_{h2} = 1$, $k_h = a_{11}b_1\|\hat{f}_h\|$, and $\varepsilon = 0.035$, then $V_h > 0$ and $\dot{V}_h < 0$ are guaranteed. The robust control input for the hydraulics, μ_h, can be obtained from (20) by setting $p(e, t) = -a_{11}b_1\dot{e}_h\|\hat{f}_h\|$.

5. Simulations

The results of computer simulations using MATLAB/SIMULINK are shown in Figs. 17–23. According to these results, the stability and velocity tracking performance of the proposed controller are better than those of a μ-controller used for the linearized system. The μ-controller was designed and analyzed by computing the structured singular value μ introduced by Doyle (1982), which is a measure of robust performance. This means that the best controller is the one that gives the best worst-case response. The worst-case is the worst combination of possible disturbances, set point changes and model errors. For this simulation, the μ-controller

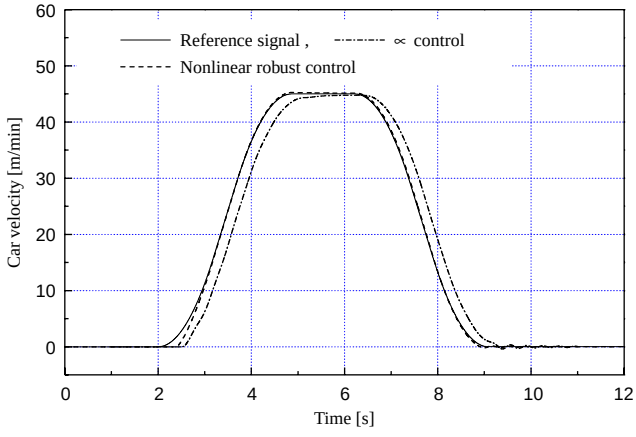

Fig. 17. Comparison of the car velocity with μ-control and nonlinear robust control: upmovement.

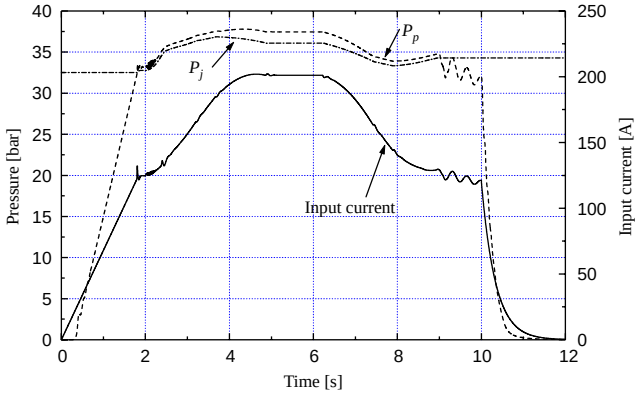

Fig. 18. The input current, pump pressure, and cylinder pressure of the nonlinear robust control in Fig. 17.

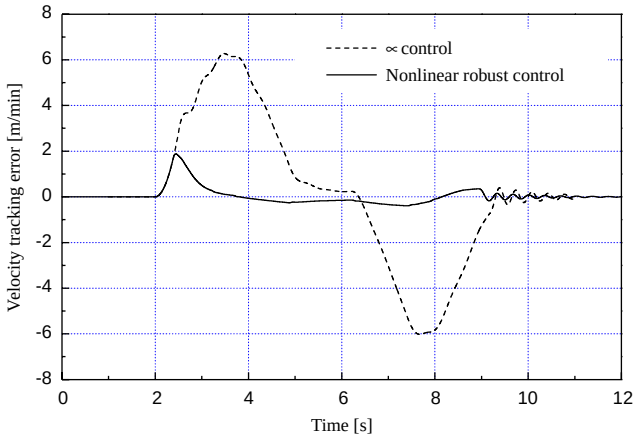

Fig. 19. Comparison of the velocity tracking errors: up movement.

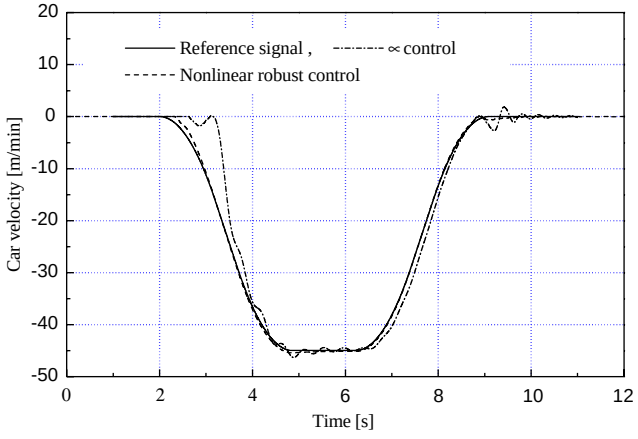

Fig. 20. Comparison of the car velocity of μ-control and nonlinear robust control: down movement.

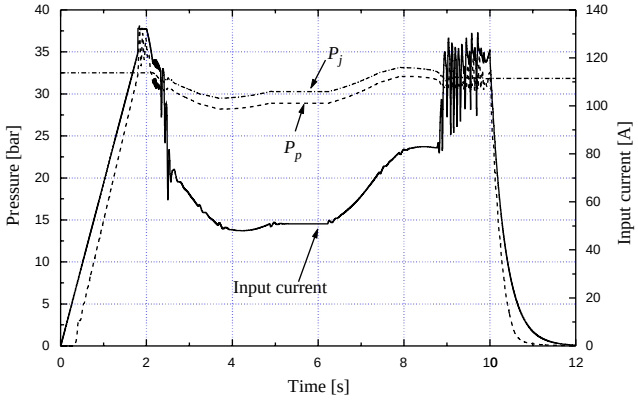

Fig. 21. The input current, pump pressure, and cylinder pressure of the nonlinear robust control in Fig. 20.

was designed according to the assumption that μ is 0.9 and that the linearized system order is reduced from 34 to 9 using the balanced reduction theorem (Kang & Kim, 2000). According to the simulation result, the maximum velocity tracking error was reduced to $\frac{1}{3}$–$\frac{1}{8}$ of

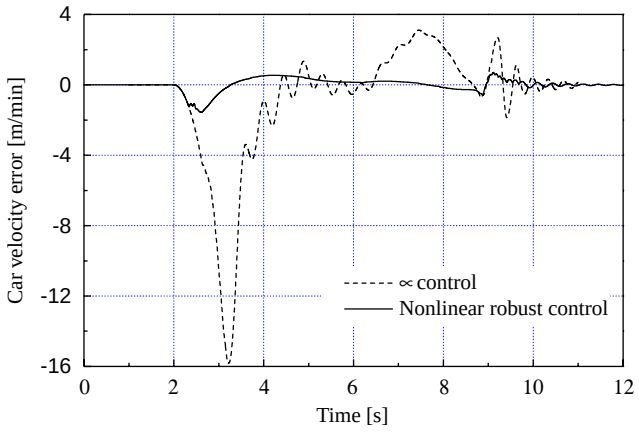

Fig. 22. Comparison of the velocity tracking errors: down movement.

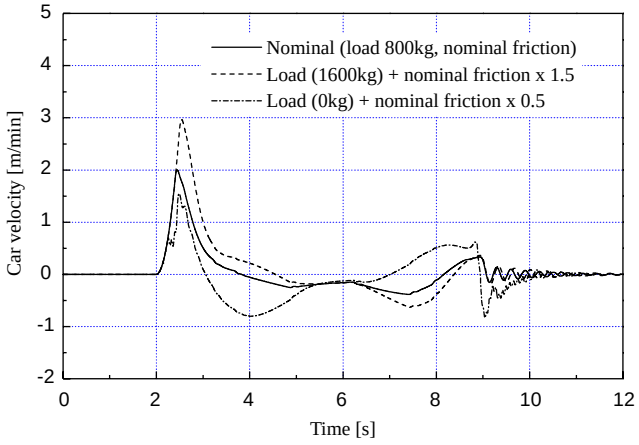

Fig. 23. Robustness in the presence of load and friction variations.

that of the μ-controller. In Figs. 18 and 21, we can see that the control input used for the simulations satisfies the pump input current specification and that the trajectories of the states are physically reasonable. The robustness was examined by changing the car's load and the magnitude of the cylinder friction. The robustness for the load and friction variations is shown in Fig. 23. Given that the load variation is ± 800 kg and the friction variation is {nominal friction} $\times 0.5 \sim$ {nominal friction} $\times 1.5$, and that the velocity tracking error is comparatively smaller than the nominal control error, the robustness of the proposed control scheme is assured.

6. Conclusions

To establish accurate simulation models and to solve the velocity tracking control problem of a hydraulic elevator system, experiment-based models for the hydraulic elevator were investigated. The dead zone

behaviors in hydraulic elevators were clarified through experiments. The mathematical models for the cylinder and pump frictions were established by combining the Karnopp's friction model and Bo and Pavelescu's friction model. The leakage at the pump was mathematically formulated by experiments resulting in a nonlinear function of temperature and pressure. To improve the performance of the velocity tracking control, a two-stage robust control using the Lyapunov redesign method was investigated. The computer simulations showed the stability and robustness of the proposed controller in the presence of nonlinearities and uncertainties. In this way, a practical methodology for designing a two-stage robust controller as well as system modeling of a hydraulic system based on experimentation were obtained.

Acknowledgements

This work was supported by the Ministry of Science and Technology of Korea under a program of the National Research Laboratory, Grant number NRL M1-0302-00-0039-03-J00-00-023-10. The authors would like to thank Prof. Kyo-Il Lee at Seoul National University for his thoughtful guidance throughout the studies at their alma mater.

Appendix A. The system matrix in (1)

In the detailed model of the mechanics in (1), see Fig. 1(b), the system matrix A_f is defined as

$$A_f = \begin{bmatrix}
0 & 1 & 0 & 0 & 0 & 0 & 0 & 0 & 0 & 0 & 0 & 0 & 0 & 0 \\
a_{2,1} & a_{2,2} & a_{2,3} & a_{2,4} & a_{2,5} & a_{2,6} & 0 & 0 & a_{2,9} & a_{2,10} & a_{2,11} & a_{2,12} & a_{2,13} & a_{2,14} \\
0 & 0 & 0 & 1 & 0 & 0 & 0 & 0 & 0 & 0 & 0 & 0 & 0 & 0 \\
a_{4,1} & a_{4,2} & a_{4,3} & a_{4,4} & a_{4,5} & a_{4,6} & a_{4,7} & a_{4,8} & a_{4,9} & a_{4,10} & 0 & 0 & 0 & 0 \\
0 & 0 & 0 & 0 & 0 & 1 & 0 & 0 & 0 & 0 & 0 & 0 & 0 & 0 \\
a_{6,1} & a_{6,2} & a_{6,3} & a_{6,4} & a_{6,5} & a_{6,6} & a_{6,7} & a_{6,8} & 0 & 0 & 0 & 0 & 0 & 0 \\
0 & 0 & 0 & 0 & 0 & 0 & 0 & 1 & 0 & 0 & 0 & 0 & 0 & 0 \\
0 & 0 & a_{8,3} & a_{8,4} & a_{8,5} & a_{8,6} & a_{8,7} & a_{8,8} & 0 & 0 & 0 & 0 & 0 & 0 \\
0 & 0 & 0 & 0 & 0 & 0 & 0 & 0 & 0 & 1 & 0 & 0 & 0 & 0 \\
a_{10,1} & a_{10,2} & a_{10,3} & a_{10,4} & a_{10,5} & a_{10,6} & 0 & 0 & a_{10,9} & a_{10,10} & 0 & 0 & 0 & 0 \\
0 & 0 & 0 & 0 & 0 & 0 & 0 & 0 & 0 & 0 & 0 & 1 & 0 & 0 \\
a_{12,1} & a_{12,2} & 0 & 0 & 0 & 0 & 0 & 0 & a_{12,9} & a_{12,10} & a_{12,11} & a_{12,12} & a_{12,13} & a_{12,14} \\
0 & 0 & 0 & 0 & 0 & 0 & 0 & 0 & 0 & 0 & 0 & 0 & 0 & 1 \\
a_{14,1} & a_{14,2} & 0 & 0 & 0 & 0 & 0 & 0 & 0 & 0 & a_{14,11} & a_{14,12} & a_{14,13} & a_{14,14}
\end{bmatrix}, \tag{A.1}$$

where

$$a_{2,1} = -(K_{j1} + K_{j2} + K_{j3} + K_{j4})/650, \quad a_{2,2} = -(C_{j1} + C_{j2} + C_{j3} + C_{j4} + C_j)/650,$$
$$a_{2,3} = K_{j1}/650, \quad a_{2,4} = C_{j1}/650, \quad a_{2,5} = K_{j1}r_{c1}/650,$$
$$a_{2,6} = C_{j1}r_{c1}/650, \quad a_{2,9} = 3.69\mathrm{e}^{-4}(-K_{j1} + K_{j2}), \quad a_{2,10} = 3.69\mathrm{e}^{-4}(-C_{j1} + C_{j2}),$$
$$a_{2,11} = 4.33\mathrm{e}^{-4}(-K_{j2} + K_{j3}), a_{2,12} = 4.33\mathrm{e}^{-4}(-C_{j2} + C_{j3}), \quad a_{2,13} = 3.69\mathrm{e}^{-4}(-K_{j3} + K_{j4}),$$
$$a_{2,14} = 3.69\mathrm{e}^{-4}(-C_{j3} + C_{j4}), a_{4,1} = K_{j1}/650, \quad a_{4,2} = C_{j1}/650,$$
$$a_{4,3} = -(K_{j1} + K_b)/1538, a_{4,4} = -(C_{j1} + C_b + C_c)/1538, \quad a_{4,5} = -1.56\mathrm{e}^{-4}K_{j1},$$
$$a_{4,6} = -1.56\mathrm{e}^{-4}C_{j1}, a_{4,7} = 1.56\mathrm{e}^{-4}K_b, \quad a_{4,8} = 1.56\mathrm{e}^{-4}C_b, \quad a_{4,9} = 1.56\mathrm{e}^{-4}K_{j1},$$
$$a_{4,10} = 1.56\mathrm{e}^{-4}C_{j1}, a_{6,1} = 0.162K_{j1}, \quad a_{6,2} = 0.162C_{j1}, \quad a_{6,3} = -0.162K_{j1},$$
$$a_{6,4} = -0.162C_{j1}, \quad a_{6,5} = -0.039(K_{j1} + K_{cb}), \quad a_{6,6} = -0.039(C_{j1} + C_{cb}),$$
$$a_{6,7} = 0.039K_{cb}, \quad a_{6,8} = 0.039C_{cb}, \quad a_{8,3} = 0.162K_c, \quad a_{8,4} = 0.162C_c, \quad a_{8,5} = 0.039K_{cb},$$

$$a_{8,6} = 0.039C_{cb}, \quad a_{8,7} = -0.039(K_{cb} + K_b), \quad a_{8,8} = -0.039(C_{cb} + C_b),$$
$$a_{10,1} = 0.162(-K_{j1} + K_{j2}), \quad a_{10,2} = 0.162(-C_{j1} + C_{j2}), \quad a_{10,3} = 0.162K_{j1},$$
$$a_{10,4} = 0.162C_{j1}, \quad a_{10,5} = 0.039K_{j1}, a_{10,6} = 0.039C_{j1}, \quad a_{10,9} = -0.039(K_{j1} + K_{j2}),$$
$$a_{10,10} = -0.039(C_{j1} + C_{j2}), \quad a_{12,1} = 0.117(-K_{j2} + K_{j3}), \quad a_{12,2} = 0.117(-C_{j2} + C_{j3}),$$
$$a_{12,9} = 0.021K_{j2}, \quad a_{12,10} = 0.021C_{j2}, \quad a_{12,11} = 0.0328(K_{j2} + K_{j3}),$$
$$a_{12,12} = -0.0328(C_{j2} + C_{j3}), \quad a_{12,13} = 0.0281K_{j3}, \quad a_{12,14} = 0.0281C_{j3},$$
$$a_{14,1} = 0.162(-K_{j3} + K_{j4}), \quad a_{14,2} = 0.162(-C_{j3} + C_{j4}), \quad a_{14,11} = 0.0493K_{j3},$$
$$a_{14,12} = 0.0493C_{j3}, \quad a_{14,13} = -0.0138(K_{j3} + K_{j4}), \text{ and } a_{14,14} = -0.0138(C_{j3} + C_{j4}).$$

As the spring constant and damping coefficient are dependant on the length of each rope segment, the following relationships are derived:

$$K_{j1} = E/L_{j1}, \quad K_{j2} = E/L_{j2}, \quad K_{j3} = E/L_{j3}, \quad K_{j4} = E/L_{j4}, \quad K_{cb} = E/L_{cb},$$
$$K_b = 1.47\mathrm{e}^5 E/L_b(E/L_b + 1.47\mathrm{e}^5), \quad E = 0.2753\mathrm{e}^{10}, \quad C_{cb} = 2\zeta\sqrt{K_{cb}M_c/2},$$
$$C_b = 2\zeta\sqrt{K_b M_c/2}, \quad C_{j1\ldots4} = 2\zeta\sqrt{K_{j1\ldots4}M_c/2}, \text{ and } \zeta = 0.07, \tag{A.2}$$

where E is obtained by Young's modulus and the cross sectional area of each rope. And the length of each rope segment is defined as follows:

$$L_{j1} = 5.23 + x_j - x_c, \quad L_{j2} = 5.939 + x_j, \quad L_{j3} = L_{j2}, \quad L_{j4} = 4.614 + x_j, \quad L_{cb} = 1.65, \text{ and } L_b = 13.64 - x_c.$$

References

Alleyne, A. (1996). Nonlinear force control of an electro-hydraulic actuator. *Japan/USA Symposium on Flexible Automation*, *1*, 193–200.

Armstrong-Helouvry, B., Dupont, P., & Wit, C. C. D. (1994). A survey of models, analysis tools and compensation method for the control of machines with friction. *Automatica*, *30*(7), 1083–1138.

Bo, L. C., & Pavelescu, D. (1982). The friction-speed relation and its influence on the critical velocity of the stick-slip motion. *Wear*, *82*(3), 277–289.

Bouri, M., & Thomasset, D. (2001). Sliding control of an electro-pneumatic actuator using an integral switching surface. *IEEE Transactions on Control Systems Technology*, *9*(2), 368–375.

Corless, M. J., & Leitmann, G. (1981). Continuous state feedback guaranteeing uniform ultimate boundedness for uncertain dynamic systems. *IEEE Transactions on Automatic Control*, *26*(5), 1139–1144.

Corless, M. J., & Leitmann, G. (1997). Componentwise bounded controllers for robust exponential convergence. *Journal of Dynamic Systems, Measurement and Control*, *119*, 73–79.

Doyle, J. C. (1982). Analysis of feedback systems with structured uncertainties. *IEEE Proc.*, *129*, 242–250.

Grognard, F., Jadot, F., Magni, L., Bastin, G., Sepulehre, R., & Wertz, V. (2001). Robust stabilization of a nonlinear cement mill model. *IEEE Transactions on Automatic Control*, *46*(4), 618–623.

Jianmin, Z. (2000). Research on speed control system of VVVF hydraulic elevator with energy feedback. *Chinese Journal of Mechanical Engineering*, *36*(7), 61–65.

Kang, K. H., & Kim, K. S. (2000). Robust velocity control for inverter-driven hydraulic elevators using DGKF/μ Approach. *Journal of Control, Automation, and Systems Engineering*, *6*(2), 217–227.

Karnopp, D. (1985). Computer simulation of stick-slip friction in mechanical dynamic systems. *Journal of Dynamic Systems, Measurement, and Control*, *107*(1), 100–103.

Khalil, H. K. (1992). *Nonlinear systems*. New York: Prentice Hall.

Kim. C.S., 2000. *A nonlinear robust control for a hydraulic elevator*. M.Sc. thesis School of Mechanical and Aerospace Engineering, Seoul National University, Korea.

Kim, H. S., Lee, K. I., & Cho, Y. M. (2002). Robust two-stage nonlinear control for a hydraulic servo-system. *International Journal of Control*, *75*(7), 502–516.

Krstic, M., Kanellakopulos, I., & Kokotovic, P. (1995). *Nonlinear and adaptive control design*. New York: Wiley.

Kwon, W. H., Han, S. H., & Ahn, C. K. (2004). Advances in nonlinear predictive control: a survey on stability and optimality. *International Journal of Control, Automation, and Systems*, *2*(1), 15–22.

Li, K. (2001). Electro-hydraulic proportional control of twin-cylinder hydraulic elevators. *Control Engineering Practice*, *9*(4), 367–373.

Michino, R., Mizumoto, I., Iwai, Z., & Kumon, M. (2003). Robust high gain adaptive output feedback control for nonlinear systems with uncertain nonlinearities in control input term. *International Journal of Control, Automation, and Systems*, *1*(1), 19–27.

Nakamura, I. (2000). Safety of hydraulic elevator. *Japan Hydraulics & Pneumatic Society*, *31*(7), 550–556.

Qu, Z. (1998). *Robust control of nonlinear uncertain systems*. New York: Wiley.

Sedrak, D. (2000). Hydraulic elevators: a look at the past, present and future. *Elevator World*, *48*(6), 100–106.

Sha, D., Bajic, V. B., & Yang, H. (2002). New model and sliding mode control of hydraulic elevator velocity tracking system. *Simulation Modeling Practice and Theory*, *9*, 365–385.

Sohl, G. A., & Bobrow, J. E. (1999). Experiments and simulations on the nonlinear control of a hydraulic servo system. *IEEE Transactions on Control Systems Technology*, *7*(2), 238–247.

Teramoto, T., & Nakamura, I. (1997). High-accuracy car level compensation device for a hydraulic elevator. *Transactions of the Japan Society of Mechanical Engineers, Series C*, *63*(611), 2321–2328.

Venkatesh, S. R., Cho, Y. M., & Kim, J. W. (2002). Robust control of vertical motions in ultra-high rise elevators. *Control Engineering Practice*, *10*(2), 121–132.

Wheeler, G., Su, C. Y., & Stepanenko, Y. (1998). A sliding mode controller with improved adaptation laws for the upper bounds on the norm of uncertainties. *Automatica*, *34*(12), 1657–1661.

Yanada, H., & Shimahara, M. (1997). Sliding mode control of an electrohydraulic servo motor using a gain scheduling type observer and controller. *Proceedings of the Institution of Mechanical Engineers Part I-Journal of Systems and Control Engineering*, *211*(6), 407–416.

Yao, B., Fanping, B., Reedy, J., & Chiu, G. (2000). Adaptive robust motion control of single-rod hydraulic actuators: theory and experiments. *IEEE-ASME Transactions on Mechatronics*, *5*(1), 79–91.